

Search for neutral MSSM Higgs bosons decaying to $\tau^+\tau^-$ pairs in proton-proton collisions at $\sqrt{s} = 7$ TeV with the ATLAS detector

The ATLAS Collaboration

Abstract

A search for neutral Higgs bosons decaying to pairs of τ leptons with the ATLAS detector at the LHC is presented. The analysis is based on proton-proton collisions at a center-of-mass energy of 7 TeV, recorded in 2010 and corresponding to an integrated luminosity of 36 pb^{-1} . After signal selection, 276 events are observed in this data sample. The observed number of events is consistent with the total expected background of 269 ± 36 events. Exclusion limits at the 95% confidence level are derived for the production cross section of a generic Higgs boson ϕ as a function of the Higgs boson mass and for $A/H/h$ production in the Minimal Supersymmetric Standard Model (MSSM) as a function of the parameters m_A and $\tan\beta$.

Keywords: Higgs boson, MSSM, tau lepton

1. Introduction

Discovering the mechanism responsible for electroweak symmetry breaking and the origin of mass for elementary particles is one of the major goals of the physics program at the Large Hadron Collider (LHC) [1]. In the Standard Model (SM) this mechanism requires the existence of a scalar particle, the Higgs boson [2, 3, 4, 5, 6]. In extensions of the Standard Model to the Minimal Supersymmetric Standard Model (MSSM) [7, 8], two Higgs doublets of opposite hypercharge are required, resulting in five observable Higgs bosons. Three of these are electrically neutral (h , H , and A) while two are charged (H^\pm). At tree level their properties such as masses, widths, and branching ratios can be predicted in terms of only two parameters, often chosen to be the mass of the CP -odd Higgs boson, m_A , and the ratio of the vacuum expectation values of the two Higgs doublets, $\tan\beta$. The Higgs boson production proceeds mainly via gluon fusion or in association with b quarks, with the latter becoming more important for large $\tan\beta$.

In this paper, a search for neutral MSSM Higgs bosons in the decay mode $A/H/h \rightarrow \tau^+\tau^-$ with the ATLAS detector [9] is presented. The decay into a $\tau^+\tau^-$ pair is a promising channel since the coupling of the Higgs bosons to third-generation fermions is strongly enhanced over large regions of the MSSM parameter space. The search considers Higgs boson decays to $e\mu 4\nu$, $e\tau_{had}3\nu$, and $\mu\tau_{had}3\nu$, where τ_{had} denotes a hadronically decaying τ lepton. These topologies have branching ratios of 6%, 23%, and 23%, respectively. This analysis is complementary to previous searches at the e^+e^- collider LEP at CERN [10] and similar to those performed at the $p\bar{p}$ collider Tevatron at Fermilab [11, 12], and extends to regions of the MSSM

parameter space untested by these machines. The CMS Collaboration has recently published results of a similar analysis [13].

2. Event samples

The data used in this search were recorded with the ATLAS detector in proton-proton collisions at a center-of-mass energy of $\sqrt{s} = 7$ TeV during the 2010 LHC run. The ATLAS detector is described in detail elsewhere [9]. In the ATLAS coordinate system, polar angles θ are measured with respect to the LHC beamline and azimuthal angles ϕ are measured in the plane transverse to the beamline. Pseudorapidities η are defined as $\eta = -\ln \tan \frac{\theta}{2}$. Transverse momenta are computed from the three-momenta p as $p_T = |p| \sin\theta$. The integrated luminosity of the data sample, considering only data-taking periods where all relevant detector subsystems were fully operational, is $36.1 \pm 1.2 \text{ pb}^{-1}$ [14]. The data were collected using a single-electron trigger with p_T threshold in the range 10–15 GeV for the $e\tau_{had}$ and $e\mu$ final states, and a single-muon trigger with p_T threshold in the range 10–13 GeV for the $\mu\tau_{had}$ final state. With respect to the signal selection described below, the total trigger efficiencies are 99% and 82% for electrons and muons, respectively. Events that pass the trigger are selected if they have a reconstructed vertex that is formed by three or more tracks and lies within 15 cm of the nominal interaction point along the beam axis.

The cross sections for Higgs boson production have been calculated using HIGLU [15] and ggh@nnlo [16] for the gluon fusion process. For the b -quark associated production, a matching scheme described in [17] is used to combine the next-to-leading order (NLO) calculation for

$gg \rightarrow b\bar{b}A/H/h$ in the 4-flavor scheme [18, 19] and the next-to-next-to-leading order (NNLO) calculation for $b\bar{b} \rightarrow A/H/h$ in the 5-flavor scheme [20]. The masses, couplings, and branching ratios of the Higgs bosons are computed with FeynHiggs [21]. The ratio of the MSSM Yukawa couplings and their SM values have been used to derive the MSSM cross sections from the respective SM cross sections. Details of the calculations and associated α_S , parton distribution function (PDF) and scale uncertainties can be found in Ref. [22]. The direct $gg \rightarrow A/H/h$ production is simulated with MC@NLO [23], and the associated $b\bar{b}A/H/h$ production with SHERPA [24]. Both $gg \rightarrow A$ and bbA samples are generated at 11 values of m_A , in the range from 90 to 300 GeV. These samples are also used for the H and h bosons assuming the same kinematics of the decay products. For any given m_A and $\tan\beta$, the masses m_H and m_h of the H and h bosons are calculated in the m_h^{max} MSSM benchmark scenario [25] and A boson events with m_A closest to m_H and m_h , respectively, are added to these samples with appropriately scaled cross sections to obtain a signal sample for $A/H/h$ production. The increase of the Higgs boson natural width with $\tan\beta$ is neglected as it is small compared with the experimental mass resolution. Table 1 shows the signal cross section times branching ratio for $\tan\beta = 40$ and $m_A = 120$ GeV.

Table 1: Cross sections for signal and background processes. For $A/H/h$ production, the cross section is multiplied by the branching ratio for $A/H/h \rightarrow \tau^+\tau^-$. The signal cross sections are given for $\tan\beta = 40$ and the three values quoted correspond to $A/H/h$ production, respectively. For $m_A = 120$ GeV and $\tan\beta = 40$, the H and h boson masses in the m_h^{max} scenario are $m_H = 131.0$ GeV and $m_h = 119.5$ GeV.

Signal process	$\sigma \times \text{BR}$ [pb]
$b\bar{b}A/H/h(\rightarrow \tau\tau), m_A = 120$ GeV	30.8/1.08/32.3
$gg \rightarrow A/H/h(\rightarrow \tau\tau), m_A = 120$ GeV	20.5/2.97/19.3
Background process	σ [pb]
$W \rightarrow \ell + \text{jets}$ ($\ell = e, \mu, \tau$)	10.46×10^3
$Z/\gamma^* \rightarrow \ell^+\ell^- + \text{jets}$ ($m_{\ell\ell} > 10$ GeV)	4.96×10^3
$t\bar{t}$	164.6
Single-top ($t-$, $s-$ and Wt -channels)	58.7, 3.9, 13.1
Di-boson (WW , WZ and ZZ)	46.2, 18.0, 5.6

Processes producing W or Z bosons that subsequently decay into leptons constitute the most important background. These processes include $W + \text{jets}$, $Z/\gamma^* + \text{jets}$, where γ^* denotes a virtual photon, top-quark ($t\bar{t}$ and single-top) and electroweak di-boson (WW , WZ , ZZ) production. Here, $Z/\gamma^* \rightarrow \tau^+\tau^- + \text{jets}$ events constitute a largely irreducible background for Higgs boson masses close to the Z boson mass. $Z/\gamma^* \rightarrow \ell^+\ell^- + \text{jets}$ ($\ell = e, \mu$) events contribute if one of the charged leptons or an accompanying jet is misidentified. Due to its large cross section, jet production in Quantum Chromodynamics (QCD) processes provides a significant background contribution if there are

real leptons from decays of heavy quarks or if jets are misidentified as electrons, muons, or hadronic τ decays.

The production of W and Z bosons in association with jets is simulated with the ALPGEN [26] and PYTHIA [27] generators. The $t\bar{t}$ and single-top processes are generated with MC@NLO, and for di-boson production HERWIG [28] and MC@NLO are used. The loop-induced process $gg \rightarrow WW$ is generated with gg2WW [29]. For events generated with ALPGEN, HERWIG, MC@NLO and gg2WW the parton shower and hadronization are simulated with HERWIG and the underlying event with JIMMY [30]. The programs TAUOLA [31, 32] and PHOTOS [33] are used to model the decays of τ leptons and the radiation of photons, respectively, in all event samples except those generated with SHERPA.

Table 1 summarizes the inclusive cross sections for the above processes, which are used to normalize the simulated event samples. The cross section for single gauge boson production is calculated at NNLO in QCD perturbation theory [34], for $t\bar{t}$ production at NLO and next-to-leading logarithms (NLL) [35, 36], and for single-top and di-boson production at NLO [23]. No simulated samples for the QCD jet background are used, as this background is entirely estimated with data. All simulated samples are processed through a full simulation of the ATLAS detector based on GEANT4 [37, 38]. To match the pile-up (overlap of several interactions in the same bunch crossing) observed in the data, minimum-bias events [39, 40] are overlaid to the generated signal and background events, and the resulting events are reweighted so that the distribution of the number of reconstructed vertices per bunch crossing agrees with the data.

3. Object reconstruction

Electron candidates are reconstructed from a cluster of energy deposits in the electromagnetic calorimeter matched to a track in the inner detector. The cluster must have a shower profile consistent with an electromagnetic shower [41]. Electron candidates are required to have a transverse momentum above 20 GeV and a pseudorapidity in the range $|\eta| < 1.37$ or $1.52 < |\eta| < 2.47$. Muon candidates are reconstructed by combining tracks in the muon spectrometer with tracks in the inner detector [41]. They must have a transverse momentum above 10 GeV and a pseudorapidity in the range $|\eta| < 2.5$ and < 2.4 in the $\ell\tau_{had}$ and $e\mu$ final states, respectively. Isolation requirements are imposed on electron (muon) candidates by requiring that the additional transverse energy in the calorimeter cells in a cone of radius $\Delta R = \sqrt{(\Delta\eta)^2 + (\Delta\phi)^2} = 0.3(0.4)$ centered on the lepton direction is less than 10% (6%) of the electron (muon) transverse energy (momentum). In addition, the sum of the transverse momenta of all tracks with $p_T > 1$ GeV within $\Delta R = 0.4$ around the lepton direction, excluding the lepton track, must be less than 6% of the lepton track transverse momentum. The reconstruction of candidates for hadronic τ decays is based on calorimeter jets re-

constructed with the anti- k_T algorithm [42, 43] with a distance parameter $R = 0.4$, seeded using three-dimensional topological calorimeter energy clusters. Their identification, including vetoing electrons and muons, is based on observables that describe the shape of the calorimeter shower and on tracking information, which are combined in a likelihood discriminator [44]. A τ candidate must have a visible transverse momentum, $p_T^{\tau,vis}$, above 20 GeV, a pseudorapidity in the range $|\eta| < 2.5$, 1 or 3 associated tracks ($p_T > 1$ GeV) and a total charge of ± 1 , computed from all tracks associated with the candidate. The efficiency of the τ identification for 1-prong (3-prong) τ candidates with $p_T^{\tau,vis} > 20$ GeV is about 65% (60%) and the probability to misidentify a jet as a τ lepton, as determined from a di-jet control sample, is about 10% (5%). When candidates fulfilling the above criteria overlap with each other geometrically (within $\Delta R < 0.2$), only one of them is selected. The overlap is resolved by selecting muons, electrons and τ candidates in this order of priority. The missing transverse momentum in the event, $E_T^{\text{miss}} = \sqrt{(E_x^{\text{miss}})^2 + (E_y^{\text{miss}})^2}$, is reconstructed as the vector sum of all topological calorimeter energy clusters in the region $|\eta| < 4.5$ and corrected for identified muons [41].

4. Event selection

The signatures of $A/H/h \rightarrow \tau^+\tau^- \rightarrow e\mu 4\nu$ signal events are one isolated electron, one isolated muon and E_T^{miss} due to the undetected neutrinos from the two τ decays. Exactly one electron with $p_T^e > 20$ GeV and one muon with $p_T^\mu > 10$ GeV with opposite electric charge are required. In order to suppress backgrounds from $t\bar{t}$, single-top and di-boson production two additional requirements are applied. The scalar sum of the transverse momentum of the electron, the transverse momentum of the muon and the missing transverse momentum must be smaller than 120 GeV, and the azimuthal opening angle between the electron and the muon must be larger than 2.0 rad.

The signatures of $A/H/h \rightarrow \tau^+\tau^-$ signal events, where one τ lepton decays leptonically and the other hadronically, are an isolated electron or muon, ℓ , a τ candidate, τ_{had} , and E_T^{miss} due to the undetected neutrinos from the two τ decays. Exactly one electron or muon with $p_T^e > 20$ GeV or $p_T^\mu > 15$ GeV and one oppositely-charged τ candidate with $p_T^{\tau,vis} > 20$ GeV are required in the event. Events with more than one electron or muon, using the lepton p_T thresholds from the object definition given in Section 3, are rejected to suppress events from $Z/\gamma^* \rightarrow \ell^+\ell^-$ ($\ell = e, \mu$) decays and from $t\bar{t}$ and single-top production. A missing transverse momentum above 20 GeV is required to reject events with jets from QCD processes as well as $Z/\gamma^* \rightarrow \ell^+\ell^-$ ($\ell = e, \mu$) decays. Events with real leptons from $W \rightarrow \ell\nu$ decays are suppressed by requiring the transverse mass of the ℓ - E_T^{miss} system, defined as

$$m_T = \sqrt{2p_T^\ell E_T^{\text{miss}}(1 - \cos \Delta\phi)}, \quad (1)$$

to be below 30 GeV. Here p_T^ℓ is the transverse momentum of the electron or muon and $\Delta\phi$ is the angle between the electron or muon and the E_T^{miss} vector in the plane perpendicular to the beam direction.

Table 2 compares the number of selected events in data with those expected from the simulation of various background processes, not including QCD jet production. After the full selection, 70, 74, and 132 data events are observed in the $e\mu$, $e\tau_{had}$, and $\mu\tau_{had}$ channels, respectively. The estimation of backgrounds based on data control samples used for the final results of the analysis is discussed in Section 5. The signal efficiency amounts to 7(3)% for $m_A = 120$ GeV and 9(8)% for $m_A = 200$ GeV in the $e\mu$ ($\ell\tau_{had}$) final states.

After the selection of signal candidates in the $e\mu$ final state, the effective mass, $m_{\tau\tau}^{\text{effective}}$, is used as the discriminating variable to search for a potential Higgs boson signal. Here, $m_{\tau\tau}^{\text{effective}}$ is calculated as the invariant mass of the electron, muon and E_T^{miss} system according to

$$m_{\tau\tau}^{\text{effective}} = \sqrt{(p_e + p_\mu + p_{\text{miss}})^2}, \quad (2)$$

where p_e and p_μ denote the four-vectors of the electron and muon, respectively, and the missing momentum four-vector is defined by $p_{\text{miss}} = (E_T^{\text{miss}}, E_x^{\text{miss}}, E_y^{\text{miss}}, 0)$.

In the $e\tau_{had}$ and $\mu\tau_{had}$ final states, the visible $\tau^+\tau^-$ mass, $m_{\tau\tau}^{\text{visible}}$, defined as the invariant mass of the electron or muon from the leptonic τ decay and the hadron(s) from the hadronic τ decay, is used as the discriminating variable.

Figure 1 shows distributions of $m_{\tau\tau}^{\text{effective}}$ and $m_{\tau\tau}^{\text{visible}}$ for the data, compared to the background expectations described in Section 5.

5. Background estimation

In the search for a Higgs boson signal the normalization and shape of the $m_{\tau\tau}^{\text{visible}}$ and $m_{\tau\tau}^{\text{effective}}$ distributions for the sum of all background contributions have to be determined. Data control samples are used, where possible, to estimate or validate the most relevant background sources: $Z/\gamma^* \rightarrow \tau^+\tau^-$ and QCD jet production in the $e\mu$ final state, and $W + \text{jets}$, $Z/\gamma^* \rightarrow \tau^+\tau^-$, and QCD jet production in the $\ell\tau_{had}$ final state. The remaining backgrounds given in Table 2 are estimated solely from simulation.

5.1. QCD jet background in the $e\mu$ final state

For the estimation of the QCD jet background, four independent samples are selected by using selection criteria on two variables: the isolation of the electron and muon and their charge product. The signal region A is defined by the selection criteria defined above, *i.e.* opposite-sign isolated leptons. Region B contains same-sign isolated leptons, region C opposite-sign anti-isolated leptons, and region D same-sign anti-isolated leptons. Anti-isolated

Table 2: Number of selected events in data and expected from Monte Carlo (MC) simulation for a data sample corresponding to 36 pb^{-1} . The total $A/H/h$ signal yields for $m_A = 120 \text{ GeV}$ and $\tan\beta = 40$ are shown in the rightmost column. Only the MC statistical uncertainties are quoted. No MC expectation is given for the QCD jet background because this background can only be reliably estimated with data (it amounts to $2.1^{+3.1}_{-2.1}$ and 7.8 ± 7.0 events for the $e\mu$ and the combined $e\tau_{had}$ and $\mu\tau_{had}$ final states, respectively, as described in Sections 5.1 and 5.2).

	Data	Total MC bkg (w/o QCD)	W +jets	Di-boson	$t\bar{t}$ + single-top	$Z/\gamma^* \rightarrow$ $ee, \mu\mu$	$Z/\gamma^* \rightarrow$ $\tau^+\tau^-$	Signal ($m_A = 120 \text{ GeV}$, $\tan\beta = 40$)
$e\mu$	70	60.4 ± 1.2	0.7 ± 0.5	2.8 ± 0.1	2.5 ± 0.1	0.8 ± 0.1	53.5 ± 1.0	16.0 ± 0.3
$e\tau_{had}$	74	72.8 ± 2.7	25.1 ± 1.8	0.37 ± 0.02	4.1 ± 0.2	10.6 ± 1.0	32.6 ± 1.8	18.7 ± 0.5
$\mu\tau_{had}$	132	145.2 ± 3.9	41.5 ± 2.1	0.59 ± 0.03	5.9 ± 0.2	11.5 ± 1.1	85.7 ± 3.1	36.6 ± 0.8

leptons are obtained by inverting the isolation criteria described in Section 3. The shape of the $m_{\tau\tau}^{\text{effective}}$ distribution in the signal region A is taken from control region C and the normalization is derived by $n_A = r_{C/D} \times n_B$. Here, n_A and n_B denote the event yields in regions A and B and $r_{C/D}$ the ratio of the event yields in regions C and D after subtracting the contribution from non-QCD jet backgrounds estimated from simulation. This method relies on the assumption that the two variables used to define the four regions are uncorrelated and that the shape of the $m_{\tau\tau}^{\text{effective}}$ distribution does not depend on the isolation or charge product requirement. This has been verified by comparing the event yields and shapes of the $m_{\tau\tau}^{\text{effective}}$ distribution in data for regions C and D and in further control regions defined by the requirement of one isolated and one non-isolated lepton.

After subtracting the contribution from non-QCD jet backgrounds, estimated from simulation, the QCD jet event yield in region B is found to be $n_B = 1.07 \pm 1.57(\text{stat.})$ and the ratio $r_{C/D}$ is determined to be $r_{C/D} = 1.97 \pm 0.12(\text{stat.})$. The QCD jet event yield in the signal region is therefore estimated to be $n_A = 2.1^{+3.1}_{-2.1}(\text{stat.})$. Systematic uncertainties are discussed in Section 6.

5.2. Background in the $\ell\tau_{had}$ final states

The method to estimate the QCD and W + jets backgrounds [45] is based on both data and simulation and uses events with same-sign charges of the electron/muon and the τ_{had} candidate. It relies on the assumptions that the shape of the $m_{\tau\tau}^{\text{visible}}$ distribution for these backgrounds is the same for opposite-sign (OS) and same-sign (SS) events and that their ratio is the same in the signal region, defined by the nominal selection, and in background-enhanced QCD and W + jets control regions. These assumptions have been verified with simulated events. The method is referred to as the baseline method and is used to derive the results for the $\ell\tau_{had}$ channel. It is cross-checked with an alternative background estimation method.

The total number of opposite-sign background events in the signal region, n_{OS}^{Bkg} , can be expressed as

$$n_{OS}^{Bkg} = n_{SS}^{Bkg} + n_{OS-SS}^{QCD} + n_{OS-SS}^W + n_{OS-SS}^Z + n_{OS-SS}^{\text{other}} \quad (3)$$

where n_{SS}^{Bkg} is the sum of all same-sign backgrounds in the signal region and the remaining terms are the differences between opposite-sign and same-sign events for the QCD, W + jets, $Z/\gamma^* \rightarrow \tau^+\tau^-$, and other backgrounds. The ratio of opposite-sign and same-sign events for the QCD background, $r_{OS/SS}^{QCD}$, is expected to be close to unity. For W + jets, a significant deviation of the ratio $r_{OS/SS}^W$ from unity is expected since W + jets production is dominated by gu/gd -processes that often give rise to a jet originating from a quark whose charge is anti-correlated with the W charge. From simulation, the ratio $r_{OS/SS}^W = 2.24 \pm 0.13(\text{stat.})$ is obtained.

Using $n_{OS-SS}^W = (r_{OS/SS}^W - 1) \cdot n_{SS}^W$ and assuming $r_{OS/SS}^{QCD} = 1$, Eq. 3 can be approximated by

$$n_{OS}^{Bkg} = n_{SS}^{Bkg} + (r_{OS/SS}^W - 1) \cdot n_{SS}^W + n_{OS-SS}^Z + n_{OS-SS}^{\text{other}} \quad (4)$$

Each of the terms in Eq. 4 is estimated separately and for each bin in the $m_{\tau\tau}^{\text{visible}}$ distribution, thus not only an estimation of the background normalization but also of the $m_{\tau\tau}^{\text{visible}}$ shape is obtained. The total number of same-sign events n_{SS}^{Bkg} is determined for the nominal selection except for changing the opposite-sign charge requirement to same-sign. In the full $m_{\tau\tau}^{\text{visible}}$ range, 36 same-sign events are selected in data. The contributions from $Z/\gamma^* \rightarrow \tau^+\tau^-$ and other backgrounds are taken from simulation: $n_{OS-SS}^Z = 112 \pm 4(\text{stat.})$ and $n_{OS-SS}^{\text{other}} = 26 \pm 2(\text{stat.})$. The W + jets term in Eq. 4 is estimated to be $(r_{OS/SS}^W - 1) \cdot n_{SS}^W = 31 \pm 2(\text{stat.})$. Here, the number of same-sign W + jets events in the signal region, n_{SS}^W , and the ratio $r_{OS/SS}^W$ are determined in a W + jets-dominated data control region selected by replacing the $m_T < 30 \text{ GeV}$ requirement in the nominal selection by $m_T > 50 \text{ GeV}$. The small contribution from backgrounds other than W + jets is subtracted based on simulation. A value of $r_{OS/SS}^W = 2.41 \pm 0.15(\text{stat.})$ is obtained. It has been checked in simulation that this ratio is approximately independent of the m_T range and can thus be used for the signal region. n_{SS}^W is obtained by scaling the number of events in the W + jets control region by the ratio of events in the signal and control regions determined from simulation. The shape of the $m_{\tau\tau}^{\text{visible}}$ distribution for this contribution is taken from simulation.

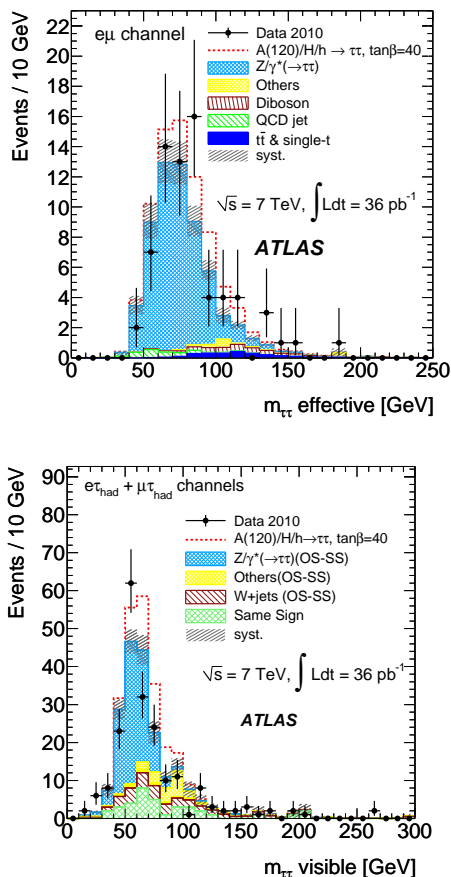


Figure 1: Effective mass distribution for the $e\mu$ final state (top) and visible mass distribution for $\ell\tau_{had}$ final states (bottom). The data are compared with the background expectation and an added hypothetical signal. “OS-SS” denotes the difference between the opposite-sign and same-sign event yields. Further explanations are given in the text.

The assumption $r_{OS/SS}^{QCD} \approx 1$ used in Eq. 4 is checked with a data control sample that is dominated by relatively low- E_T jets from QCD processes, as expected in the signal region. This sample is selected by replacing the requirement $E_T^{miss} > 20$ GeV with $E_T^{miss} < 15$ GeV and relaxing the isolation of the electron/muon candidate. After subtraction of the other backgrounds using simulation, a value of $r_{OS/SS}^{QCD} = 1.16 \pm 0.04(stat.)$ is obtained. The observed deviation of $r_{OS/SS}^{QCD}$ from unity is taken into account in the determination of systematic uncertainties for the final result, leading to a total systematic uncertainty of 19% on $r_{OS/SS}^{QCD}$. This uncertainty also includes an uncertainty associated with the dependence of $r_{OS/SS}^{QCD}$ on the lepton isolation and detector effects.

The total background estimate obtained from Eq. 4 is $n_{OS}^{Bkg} = 206 \pm 7(stat.)$, to be compared with 206 events observed in data.

An alternative background estimation is performed, which provides separate estimates of the QCD and W +jets background contributions and is used to cross-check the

results of the baseline method discussed before. For the QCD jet background the same method and assumptions as described in Section 5.1 for the $e\mu$ final state are used, but replacing one of the leptons (e or μ) by the τ_{had} candidate and using the $m_{\tau\tau}^{visible}$ distribution instead of $m_{\tau\tau}^{effective}$. The shape of the $m_{\tau\tau}^{visible}$ distribution is taken from region B and scaled by the ratio of event yields in regions C and D: $r_{C/D} = 1.12 \pm 0.04(stat.)$. The resulting estimate of the QCD jet background in the signal region is $n_A^{QCD} = r_{C/D} \times n_B = 7.8 \pm 7.0(stat.)$. The estimate of the W +jets background is obtained by deriving a scale factor of $0.83 \pm 0.04(stat.)$ for the normalization of the simulated $m_{\tau\tau}^{visible}$ distribution in a W -dominated data control sample. This control region is defined by replacing the $m_T < 30$ GeV requirement in the nominal selection by $70 < m_T < 120$ GeV. The shape of the W +jets background is taken from simulation. The estimated number of W +jets events for the nominal selection amounts to $54.8 \pm 2.1(stat.)$ events. Adding the expected number of events for $Z/\gamma^* \rightarrow \tau^+\tau^-$ and the other backgrounds from simulation (see Table 2) to the sum of the estimated QCD jet and W +jets yields, a total background contribution of $211 \pm 8(stat.)$ events is obtained, which agrees well with the 206 events observed in data. The $m_{\tau\tau}^{visible}$ shapes predicted by the two methods are found to agree as well.

5.3. Validation of the $Z/\gamma^* \rightarrow \tau^+\tau^-$ background shape

The shape of the $m_{\tau\tau}^{visible}$ and $m_{\tau\tau}^{effective}$ distributions for the irreducible $Z/\gamma^* \rightarrow \tau^+\tau^-$ background can be determined from a high-purity data sample of $Z/\gamma^* \rightarrow \mu^+\mu^-$ events in which the muons are removed and replaced by simulated τ leptons. Thus, only the τ decays and the corresponding detector response are taken from simulation, whereas the underlying Z/γ^* kinematics and all other properties of the event are obtained from the $Z/\gamma^* \rightarrow \mu^+\mu^-$ data. Figure 2 compares the $m_{\tau\tau}^{visible}$ and $m_{\tau\tau}^{effective}$ distributions of the τ -embedded sample with simulated $Z/\gamma^* \rightarrow \tau^+\tau^-$ events. A good agreement is observed within the sizable statistical uncertainties, justifying the use of the simulation for the determination of the $Z/\gamma^* \rightarrow \tau^+\tau^-$ background. This background is normalized according to the theoretical cross section in Table 1, which agrees with the ATLAS $Z/\gamma^* \rightarrow \ell^+\ell^-$ cross section measurement [41].

6. Systematic uncertainties

Systematic effects on the signal efficiency and the estimated number of background events are evaluated. The uncertainties can be grouped in four categories: theoretical inclusive cross sections, acceptance, knowledge of detector performance and systematic uncertainties of the data-driven approaches to estimate the background contribution.

The uncertainty on the theoretical inclusive cross section for each individual signal and background process is

Table 3: Uncertainties on the number of selected events for those background contributions that are at least partially estimated from simulation and for a hypothetical signal ($m_A = 120$ GeV). All numbers are given in %. When two numbers are given the first refers to the $e\mu$ final state and the second to the $\ell\tau_{had}$ final states. If an uncertainty does not apply for a certain background, this is indicated by a “-”.

	W +jets	Di-boson	$t\bar{t}$ + single-top	$Z/\gamma^* \rightarrow$ $ee, \mu\mu$	$Z/\gamma^* \rightarrow$ $\tau^+\tau^-$	Signal ($m_A = 120$ GeV, $\tan\beta = 40$)
σ_{theory}	5/-	7	10	5	5	14
Acceptance	3/-	1/2	5/2	2/14	3/14	5/4-7
e efficiency	8/-	7/3	7/3	9/2	8/7	7/6
μ efficiency	2/-	2/2	2/2	2/2	2/2	2/2
τ efficiency and fake rate	-/-	-/4	-/4	-/20	-/4	-/4
Energy scales and resolutions	2/-	2/2	4/2	2/28	2/36	1/19
Luminosity	3.4/-	3.4	3.4	3.4	3.4	3.4
Total uncertainty	11/-	11/9	15/12	11/38	11/40	16/25

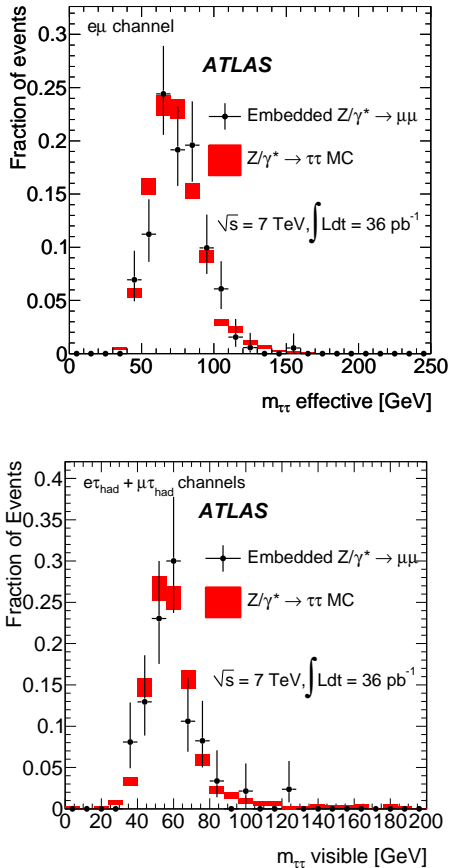


Figure 2: Effective mass distribution for the $e\mu$ final state (top) and visible mass distribution for the $\ell\tau_{had}$ final states (bottom) for simulated $Z/\gamma^* \rightarrow \tau^+\tau^-$ events (boxes) and τ -embedded $Z/\gamma^* \rightarrow \mu^+\mu^-$ events (points) passing the signal selection. The size of the boxes and the length of the error bars indicate the statistical uncertainty on the simulated and τ -embedded sample, respectively.

obtained from variations of the renormalization and factorization scales (μ_R, μ_F) by factors 1/2 and 2 and a variation of the strong coupling constant and the PDF sets within their uncertainties. The uncertainty on the acceptance is estimated by varying μ_R, μ_F , matching parameters in ALPGEN and the choice of the PDF in the generation of simulated event samples. The uncertainty on the trigger efficiencies for electrons and muons is 1%. The uncertainties due to the limited knowledge of the detector performance are evaluated by varying the trigger, reconstruction and identification efficiencies for electrons, muons and τ candidates, and by varying the energy resolution and energy scale of electrons, muons, τ candidates, and energy deposits outside of these objects. These are propagated in a fully correlated way into the E_T^{miss} scale and resolution. For the probability to misidentify electrons as τ candidates, a 20% uncertainty is assumed, resulting in a 20% uncertainty on the $Z/\gamma^* \rightarrow e^+e^-$ background.

The size of the uncertainties from the different sources on the various background processes which are at least partially estimated from simulated events are summarized in Table 3. The luminosity uncertainty is 3.4%.

The dominant systematic uncertainty in the $\ell\tau_{had}$ final states is due to the variation of the jet and τ energy scales, which are dependent on transverse momentum and pseudorapidity, by typically 7% and 5%, respectively. The difference in the impact of the energy scale and resolution uncertainty on the expected event yields in the $\ell\tau_{had}$ and $e\mu$ final states is caused by requiring a hadronic τ decay with $p_T^{\tau,vis} > 20$ GeV and a lower threshold $E_T^{miss} > 20$ GeV in the $\ell\tau_{had}$ final states, whereas in the $e\mu$ final state only an upper threshold of $p_T^e + p_T^\mu + E_T^{miss} < 120$ GeV is required. The uncertainties, apart from the ones related to the data-driven techniques, are treated as fully correlated between the three final states.

The systematic uncertainty from the data-driven estimate of the QCD jet background in the $e\mu$ final state corresponds to 0.8 events. It includes the systematic uncertainty on the subtracted non-QCD background (0.2 events) and on the assumption of identical $m_{\tau\tau}^{effective}$ shapes in

the different control regions (uncertainty on $r_{C/D}$ of 0.78). The final estimate for the QCD jet yield in the signal region is therefore $n_A = 2.1_{-2.1}^{+3.1}(\text{stat.}) \pm 0.8(\text{syst.}) = 2.1_{-2.1}^{+3.2}$. The total uncertainty is dominated by the small event yield in control region B.

For the $\ell\tau_{had}$ channels, the most important uncertainties for the data-driven estimation of the QCD jet and W + jets backgrounds (see Eq. 4) are the statistical uncertainty on the number of same-sign events in the signal region (17%) and the uncertainty on the ratios $r_{OS/SS}^{\text{QCD}}$ (19%) and $r_{OS/SS}^W$ (11%). An additional uncertainty of 10% is derived from the m_T dependence of $r_{OS/SS}^W$, *i.e.* for the extrapolation from control to signal region. The final estimate for the total background yield is $n_{OS}^{Bkg} = 206 \pm 7(\text{stat.}) \pm 34(\text{syst.}) = 206 \pm 35$.

The impact of the energy scale uncertainties of the electron, muon, τ candidate, and E_T^{miss} on the shapes of the discriminating mass variables are included as an additional correlated uncertainty in the derivation of the Higgs boson exclusion limits in Section 7. All other systematic uncertainties have no significant effect on the mass shape.

Combining the estimated contribution from the various background processes and their uncertainties results in the final background estimate shown in Table 4.

Table 4: Observed numbers of events in data, for an integrated luminosity of 36 pb^{-1} , and total expected background contributions for the final states considered in this analysis, with their combined statistical and systematic uncertainties.

Final state	Exp. Background	Data
$e\mu$	63 ± 7	70
$\ell\tau_{had}$	206 ± 35	206
Sum	269 ± 36	276

7. Results

No significant excess of events is observed in the data, compared to the SM expectation. Exclusion limits at the 95% confidence level are set on the production cross section times branching ratio of a generic Higgs boson ϕ as a function of its mass and for MSSM Higgs boson $A/H/h$ production as a function of the parameters m_A and $\tan\beta$. The exclusion limits are derived with the profile likelihood method [46] from an analysis of the $m_{\tau\tau}^{\text{effective}}$ distribution for the $e\mu$ final state and the $m_{\tau\tau}^{\text{visible}}$ distribution for the $\ell\tau_{had}$ final states.

Systematic uncertainties are separated into common, fully correlated (energy scale, acceptance, luminosity) and channel-specific, and are included as nuisance parameters. The $m_{\tau\tau}^{\text{effective}}$ and $m_{\tau\tau}^{\text{visible}}$ shape uncertainties due to variation of the energy scales of leptons and E_T^{miss} for the backgrounds obtained from simulation are taken into account.

The p -values for the consistency of the observed data with the background-only hypothesis range from 3% for a mass of 300 GeV to 59% for a mass of 110 GeV for the combination of the $e\mu$ and $\ell\tau_{had}$ channels.

Background-only toy MC experiments are generated to find the median expected limit along with the $\pm 1\sigma$ and $+2\sigma$ error bands. As a protection against excluding the signal hypothesis in cases of downward fluctuations of the background, the observed limit is not allowed to fluctuate below -1σ of the expected limit, *i.e.* a power-constrained limit (PCL, [47]), with the power required to be larger than 16%, is given.

Figure 3 shows the resulting exclusion limits. The cross section limit is evaluated for signal acceptances of two different production processes, $gg \rightarrow \phi$ and b-quark associated production, where ϕ denotes a generic neutral Higgs boson. Differences in the observed limits for the two processes are small compared to the 1σ error and occur due to differences in the signal shapes used in the extraction of the limits. The limit on the production cross section times branching ratio into a pair of τ leptons for a generic Higgs boson ϕ is in the range between approximately 300 pb for a Higgs boson mass of 90 GeV and approximately 10 pb for a Higgs boson mass of 300 GeV, with a small dependence on the production mode considered. The limit on the production of neutral MSSM Higgs bosons $A/H/h$ in the $\tan\beta - m_A$ plane, also shown in Figure 3, uses the m_h^{max} scenario and Higgsino mass parameter $\mu > 0$.

8. Conclusions

In this paper, a search for neutral MSSM Higgs bosons $A/H/h$ with the ATLAS detector in proton-proton collisions corresponding to an integrated luminosity of 36 pb^{-1} at a center-of-mass energy of 7 TeV is presented. Candidates for $A/H/h \rightarrow \tau^+\tau^-$ decays are selected in the three final states $e\mu$, $e\tau_{had}$, and $\mu\tau_{had}$. No evidence for a Higgs boson signal is observed in the reconstructed mass spectra. Exclusion limits on both, the cross section for the production of a generic Higgs boson ϕ as a function of its mass and on MSSM Higgs boson production $A/H/h$ as a function of m_A and $\tan\beta$, are derived. These results exclude regions of parameters space beyond the existing limits from previous experiments at LEP and the Tevatron and are similar to those recently obtained by the CMS Collaboration.

9. Acknowledgements

We thank CERN for the very successful operation of the LHC, as well as the support staff from our institutions without whom ATLAS could not be operated efficiently.

We acknowledge the support of ANPCyT, Argentina; YerPhI, Armenia; ARC, Australia; BMWF, Austria; ANAS, Azerbaijan; SSTC, Belarus; CNPq and FAPESP, Brazil; NSERC, NRC and CFI, Canada; CERN; CONICYT, Chile;

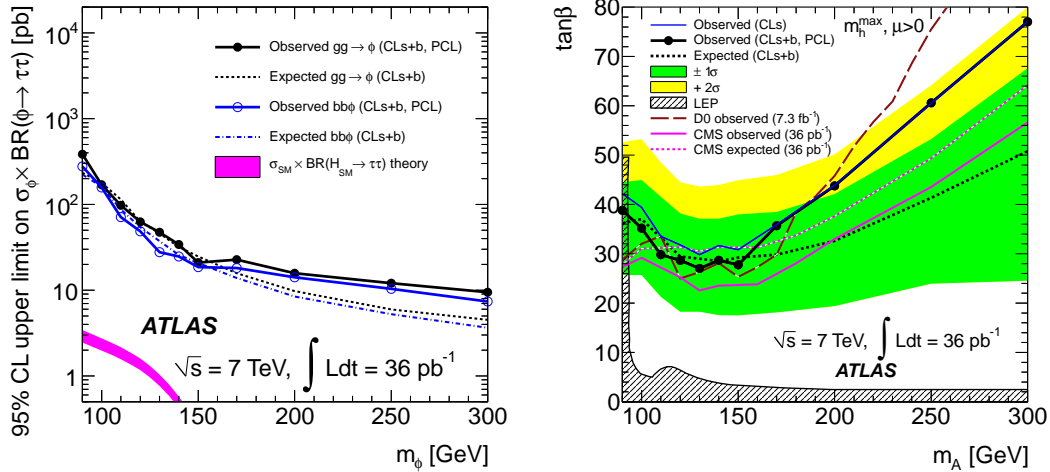


Figure 3: Left: Expected and observed limits on the production cross section and branching ratio for a generic Higgs boson ϕ , $\sigma_\phi \times BR(\phi \rightarrow \tau^+ \tau^-)$, at the 95% confidence level, as a function of the Higgs boson mass for both production modes considered. The solid and dashed lines show the observed and expected exclusion limits, respectively. For comparison the SM cross section, $\sigma_{SM} \times BR(H_{SM} \rightarrow \tau^+ \tau^-)$, is also shown. Right: Expected and observed exclusion limits in the $m_A - \tan\beta$ plane of the MSSM. The region above the drawn limit curve is excluded at the 95% confidence level. The dark grey (green) and light grey (yellow) bands correspond to the $\pm 1\sigma$ and $+2\sigma$ error bands, respectively. For comparison the observed limit based on CL_s [48, 49] is shown in addition to the one based on CL_{s+b} . The observed limit is shown up to $\tan\beta \approx 80$ although it should be noted that the region $\tan\beta > 65$ is considered to be theoretically not well under control [50]. The exclusion limits from LEP, D0, and CMS are also shown.

CAS, MOST and NSFC, China; COLCIENCIAS, Colombia; MSMT CR, MPO CR and VSC CR, Czech Republic; D NRF, DNSRC and Lundbeck Foundation, Denmark; ARTEMIS, European Union; IN2P3-CNRS, CEA-DSM/IRFU, France; GNAS, Georgia; BMBF, DFG, HGF, MPG and AvH Foundation, Germany; GSRT, Greece; ISF, MINERVA, GIF, DIP and Benoziyo Center, Israel; INFN, Italy; MEXT and JSPS, Japan; CNRST, Morocco; FOM and NWO, Netherlands; RCN, Norway; MNiSW, Poland; GRICES and FCT, Portugal; MERYS (MECTS), Romania; MES of Russia and ROSATOM, Russian Federation; JINR; MSTU, Serbia; MSSR, Slovakia; ARRS and MVZT, Slovenia; DST/NRF, South Africa; MICINN, Spain; SRC and Wallenberg Foundation, Sweden; SER, SNSF and Cantons of Bern and Geneva, Switzerland; NSC, Taiwan; TAEK, Turkey; STFC, the Royal Society and Leverhulme Trust, United Kingdom; DOE and NSF, United States of America.

The crucial computing support from all WLCG partners is acknowledged gratefully, in particular from CERN and the ATLAS Tier-1 facilities at TRIUMF (Canada), NDGF (Denmark, Norway, Sweden), CC-IN2P3 (France), KIT/GridKA (Germany), INFN-CNAF (Italy), NL-T1 (Netherlands), PIC (Spain), ASGC (Taiwan), RAL (UK) and BNL (USA) and in the Tier-2 facilities worldwide.

References

- [1] L. Evans and P. Bryant, JINST 3 (2008) S08001.
- [2] F. Englert and R. Brout, Phys. Rev. Lett. 13 (1964) 321.
- [3] P. W. Higgs, Phys. Lett. 12 (1964) 132.
- [4] P. W. Higgs, Phys. Rev. Lett. 13 (1964) 508.
- [5] P. W. Higgs, Phys. Rev. 145 (1966) 1156.
- [6] G. S. Guralnik, C.R. Hagen and T. W. B. Kibble, Phys. Rev. Lett. 13 (1964) 585.
- [7] H. P. Nilles, Phys. Rep. 110 (1984) 1.
- [8] H. E. Haber and G. L. Kane, Phys. Rep. 117 (1985) 75.
- [9] The ATLAS Collaboration, JINST 3 (2008) S08003.
- [10] ALEPH, DELPHI, L3 and OPAL Collaborations and LEP Working Group for Higgs Boson Searches, S. Schael et al., Eur. Phys. J. C47 (2006) 547.
- [11] The CDF and D0 Collaborations and Tevatron New Physics Higgs Working Group (TEVNPBWG), arXiv:1003.3363[hep-ex].
- [12] The D0 Collaboration, V.M. Abazov et al., arXiv:1106.4885[hep-ex].
- [13] The CMS Collaboration, S. Chatrchyan et al., arXiv:1104.1619[hep-ex].
- [14] The ATLAS Collaboration, ATLAS-CONF-2011-011.
- [15] M. Spira, hep-ph/9510347.
- [16] R. Harlander and W. B. Kilgore, Phys. Rev. Lett. 88 (2002) 201801.
- [17] R. Harlander, M. Krämer and M. Schumacher, CERN-PH-TH/2011-134 - FR-PHENO-2011-009 - TTK-11-17 - WUB/11-04, <https://twiki.cern.ch/twiki/pub/LHCPhysics/MSSMNeutral/santandermatching-hks.pdf>.
- [18] S. Dittmaier, M. Kramer and M. Spira, Phys. Rev. D70 (2004) 074010.
- [19] S. Dawson, C. B. Jackson, L. Reina and D. Wackerroth, Mod. Phys. Lett. A21 (2006) 89.
- [20] R. Harlander and W. B. Kilgore, Phys. Rev. D68 (2003) 013001.
- [21] M. Frank et al., JHEP 0702 (2007) 047.
- [22] The LHC Higgs Cross Section Working Group, S. Dittmaier, C. Mariotti, G. Passarino, R. Tanaka (Eds.) et al., arXiv:1101.0593[hep-ph].
- [23] S. Frixione and B. R. Webber, JHEP 06 (2002) 029.
- [24] T. Gleisberg et al., JHEP 02 (2009) 007.
- [25] M. Carena, S. Heinemeyer, C. E. M. Wagner, and G. Weiglein, Eur. Phys. J. C26 (2003) 601.
- [26] M. L. Mangano et al., JHEP 07 (2003) 001.
- [27] T. Sjöstrand, S. Mrenna and P. Skands, JHEP 05 (2006) 026.
- [28] G. Corcella et al., JHEP 01 (2001) 010.
- [29] T. Binoth, M. Ciccolini, N. Kauer and M. Kramer, JHEP 12 (2006) 046.
- [30] J. M. Butterworth, J. R. Forshaw and M. H. Seymour, Z. Phys. C72 (1996) 637.

- [31] S. Jadach, Z. Was, R. Decker and J. H. Kuhn, *Comput. Phys. Commun.* 76 (1993) 361.
- [32] P. Golonka, B. Kersevan, T. Pierzchala, E. Richter-Was, Z. Was and M. Worek, *Comput. Phys. Commun.* 174 (2006) 818.
- [33] E. Barberio and Z. Was, *Comput. Phys. Commun.* 79 (1994) 291.
- [34] R. Gavin, Y. Li, F. Petriello and S. Quackenbush, [arXiv:1011.3540](https://arxiv.org/abs/1011.3540) [[hep-ph](https://arxiv.org/abs/1011.3540)].
- [35] S. Moch and P. Uwer, *Nucl. Phys. Proc. Suppl.* 183 (2008) 75.
- [36] U. Langenfeld, S. Moch and P. Uwer, [arXiv:0907.2527](https://arxiv.org/abs/0907.2527) [[hep-ph](https://arxiv.org/abs/0907.2527)].
- [37] The GEANT4 Collaboration, S. Agostinelli et al., *Nucl. Instrum. Meth. A*506 (2003) 250.
- [38] The ATLAS Collaboration, *Eur. Phys. J. C*70 (2010) 823.
- [39] The ATLAS Collaboration, [ATL-PHYS-PUB-2010-014](https://arxiv.org/abs/2010.014).
- [40] The ATLAS Collaboration, [ATLAS-CONF-2010-031](https://arxiv.org/abs/2010.031).
- [41] The ATLAS Collaboration, *JHEP* 12 (2010) 060.
- [42] M. Cacciari, G. P. Salam and G. Soyez, *JHEP* 04 (2008) 063.
- [43] M. Cacciari and G. P. Salam, *Phys. Lett. B* 641 (2006) 57.
- [44] The ATLAS Collaboration, [ATLAS-CONF-2011-077](https://arxiv.org/abs/2011.077).
- [45] The ATLAS Collaboration, [ATLAS-CONF-2010-096](https://arxiv.org/abs/2010.096).
- [46] G. Cowan, K. Cranmer, E. Gross and O. Vitells, *Eur. Phys. J. C*71 (2011) 1554.
- [47] G. Cowan, K. Cranmer, E. Gross and O. Vitells, [arXiv:1105.3166](https://arxiv.org/abs/1105.3166) [[physics.data-an](https://arxiv.org/abs/1105.3166)].
- [48] T. Junk, *Nucl. Instrum. Meth. A*434 (1999) 435.
- [49] A. L. Read, *J. Phys. G*28 (2002) 2693.
- [50] A. Djouadi, *Phys. Rep.* 459 (2008) 1.

H. Wang^{32b,aa}, J. Wang¹⁵¹, J. Wang^{32d}, J.C. Wang¹³⁸, R. Wang¹⁰³, S.M. Wang¹⁵¹, A. Warburton⁸⁵, C.P. Ward²⁷, M. Warsinsky⁴⁸, P.M. Watkins¹⁷, A.T. Watson¹⁷, M.F. Watson¹⁷, G. Watts¹³⁸, S. Watts⁸², A.T. Waugh¹⁵⁰, B.M. Waugh⁷⁷, J. Weber⁴², M. Weber¹²⁹, M.S. Weber¹⁶, P. Weber⁵⁴, A.R. Weidberg¹¹⁸, P. Weigell⁹⁹, J. Weingarten⁵⁴, C. Weiser⁴⁸, H. Wellenstein²², P.S. Wells²⁹, M. Wen⁴⁷, T. Wenaus²⁴, S. Wendler¹²³, Z. Weng^{151,q}, T. Wengler²⁹, S. Wenig²⁹, N. Wermes²⁰, M. Werner⁴⁸, P. Werner²⁹, M. Werth¹⁶³, M. Wessels^{58a}, C. Weydert⁵⁵, K. Whalen²⁸, S.J. Wheeler-Ellis¹⁶³, S.P. Whitaker²¹, A. White⁷, M.J. White⁸⁶, S. White²⁴, S.R. Whitehead¹¹⁸, D. Whiteson¹⁶³, D. Whittington⁶¹, F. Wicek¹¹⁵, D. Wicke¹⁷⁴, F.J. Wickens¹²⁹, W. Wiedenmann¹⁷², M. Wielers¹²⁹, P. Wienemann²⁰, C. Wiglesworth⁷⁵, L.A.M. Wiik⁴⁸, P.A. Wijeratne⁷⁷, A. Wildauer¹⁶⁷, M.A. Wildt^{41,o}, I. Wilhelm¹²⁶, H.G. Wilkens²⁹, J.Z. Will⁹⁸, E. Williams³⁴, H.H. Williams¹²⁰, W. Willis³⁴, S. Willocq⁸⁴, J.A. Wilson¹⁷, M.G. Wilson¹⁴³, A. Wilson⁸⁷, I. Wingerter-Seez⁴, S. Winkelmann⁴⁸, F. Winklmeier²⁹, M. Wittgen¹⁴³, M.W. Wolter³⁸, H. Wolters^{124a,h}, G. Wooden¹¹⁸, B.K. Wosiek³⁸, J. Wotschack²⁹, M.J. Woudstra⁸⁴, K. Wraight⁵³, C. Wright⁵³, B. Wrona⁷³, S.L. Wu¹⁷², X. Wu⁴⁹, Y. Wu^{32b,ab}, E. Wulf³⁴, R. Wunstorff⁴², B.M. Wynne⁴⁵, L. Xaplanteris⁹, S. Xella³⁵, S. Xie⁴⁸, Y. Xie^{32a}, C. Xu^{32b,ac}, D. Xu¹³⁹, G. Xu^{32a}, B. Yabsley¹⁵⁰, S. Yacoub^{145b}, M. Yamada⁶⁶, A. Yamamoto⁶⁶, K. Yamamoto⁶⁴, S. Yamamoto¹⁵⁵, T. Yamamura¹⁵⁵, J. Yamaoka⁴⁴, T. Yamazaki¹⁵⁵, Y. Yamazaki⁶⁷, Z. Yan²¹, H. Yang⁸⁷, U.K. Yang⁸², Y. Yang⁶¹, Y. Yang^{32a}, Z. Yang^{146a,146b}, S. Yanush⁹¹, W-M. Yao¹⁴, Y. Yao¹⁴, Y. Yasu⁶⁶, G.V. Ybeles Smit¹³⁰, J. Ye³⁹, S. Ye²⁴, M. Yilmaz^{3c}, R. Yoosoofmiya¹²³, K. Yorita¹⁷⁰, R. Yoshida⁵, C. Young¹⁴³, S. Youssef²¹, D. Yu²⁴, J. Yu⁷, J. Yu^{32c,ac}, L. Yuan^{32a,ad}, A. Yurkewicz¹⁴⁸, V.G. Zaets¹²⁸, R. Zaidan⁶³, A.M. Zaitsev¹²⁸, Z. Zajacova²⁹, Yo.K. Zalite¹²¹, L. Zanello^{132a,132b}, P. Zarzhitsky³⁹, A. Zaytsev¹⁰⁷, C. Zeitnitz¹⁷⁴, M. Zeller¹⁷⁵, A. Zemla³⁸, C. Zender²⁰, O. Zenin¹²⁸, T. Ženiš^{144a}, Z. Zenonos^{122a,122b}, S. Zenz¹⁴, D. Zerwas¹¹⁵, G. Zevi della Porta⁵⁷, Z. Zhan^{32d}, D. Zhang^{32b,aa}, H. Zhang⁸⁸, J. Zhang⁵, X. Zhang^{32d}, Z. Zhang¹¹⁵, L. Zhao¹⁰⁸, T. Zhao¹³⁸, Z. Zhao^{32b}, A. Zhemchugov⁶⁵, S. Zheng^{32a}, J. Zhong^{151,ae}, B. Zhou⁸⁷, N. Zhou¹⁶³, Y. Zhou¹⁵¹, C.G. Zhu^{32d}, H. Zhu⁴¹, J. Zhu⁸⁷, Y. Zhu¹⁷², X. Zhuang⁹⁸, V. Zhuravlov⁹⁹, D. Zieminska⁶¹, R. Zimmermann²⁰, S. Zimmermann²⁰, S. Zimmermann⁴⁸, M. Ziolkowski¹⁴¹, R. Zitoun⁴, L. Živković³⁴, V.V. Zmouchko^{128,*}, G. Zobernig¹⁷², A. Zoccoli^{19a,19b}, Y. Zolnierowski⁴, A. Zsenei²⁹, M. zur Nedden¹⁵, V. Zutshi¹⁰⁶, L. Zwalinski²⁹.

¹ University at Albany, Albany NY, United States of America

² Department of Physics, University of Alberta, Edmonton AB, Canada

³ (a) Department of Physics, Ankara University, Ankara; (b) Department of Physics, Dumlupinar University, Kutahya; (c) Department of Physics, Gazi University, Ankara; (d) Division of Physics, TOBB University of Economics and Technology, Ankara; (e) Turkish Atomic Energy Authority, Ankara, Turkey

⁴ LAPP, CNRS/IN2P3 and Université de Savoie, Annecy-le-Vieux, France

⁵ High Energy Physics Division, Argonne National Laboratory, Argonne IL, United States of America

⁶ Department of Physics, University of Arizona, Tucson AZ, United States of America

⁷ Department of Physics, The University of Texas at Arlington, Arlington TX, United States of America

⁸ Physics Department, University of Athens, Athens, Greece

⁹ Physics Department, National Technical University of Athens, Zografou, Greece

¹⁰ Institute of Physics, Azerbaijan Academy of Sciences, Baku, Azerbaijan

¹¹ Institut de Física d'Altes Energies and Universitat Autònoma de Barcelona and ICREA, Barcelona, Spain

¹² (a) Institute of Physics, University of Belgrade, Belgrade; (b) Vinca Institute of Nuclear Sciences, Belgrade, Serbia

¹³ Department for Physics and Technology, University of Bergen, Bergen, Norway

¹⁴ Physics Division, Lawrence Berkeley National Laboratory and University of California, Berkeley CA, United States of America

¹⁵ Department of Physics, Humboldt University, Berlin, Germany

¹⁶ Albert Einstein Center for Fundamental Physics and Laboratory for High Energy Physics, University of Bern, Bern, Switzerland

¹⁷ School of Physics and Astronomy, University of Birmingham, Birmingham, United Kingdom

¹⁸ (a) Department of Physics, Bogazici University, Istanbul; (b) Division of Physics, Dogus University, Istanbul;

(c) Department of Physics Engineering, Gaziantep University, Gaziantep; (d) Department of Physics, Istanbul Technical University, Istanbul, Turkey

¹⁹ (a) INFN Sezione di Bologna; (b) Dipartimento di Fisica, Università di Bologna, Bologna, Italy

²⁰ Physikalisches Institut, University of Bonn, Bonn, Germany

²¹ Department of Physics, Boston University, Boston MA, United States of America

²² Department of Physics, Brandeis University, Waltham MA, United States of America

²³ (a) Universidade Federal do Rio De Janeiro COPPE/EE/IF, Rio de Janeiro; (b) Federal University of Juiz de Fora (UFJF), Juiz de Fora, Brazil; (c) Federal University of Sao Joao del Rei (UFSJ), Sao Joao del Rei, Brazil; (d) Instituto de Fisica, Universidade de Sao Paulo, Sao Paulo, Brazil

²⁴ Physics Department, Brookhaven National Laboratory, Upton NY, United States of America

²⁵ ^(a)National Institute of Physics and Nuclear Engineering, Bucharest; ^(b)University Politehnica Bucharest, Bucharest;
^(c)West University in Timisoara, Timisoara, Romania
²⁶ Departamento de Física, Universidad de Buenos Aires, Buenos Aires, Argentina
²⁷ Cavendish Laboratory, University of Cambridge, Cambridge, United Kingdom
²⁸ Department of Physics, Carleton University, Ottawa ON, Canada
²⁹ CERN, Geneva, Switzerland
³⁰ Enrico Fermi Institute, University of Chicago, Chicago IL, United States of America
³¹ ^(a)Departamento de Física, Pontificia Universidad Católica de Chile, Santiago; ^(b)Departamento de Física, Universidad Técnica Federico Santa María, Valparaíso, Chile
³² ^(a)Institute of High Energy Physics, Chinese Academy of Sciences, Beijing; ^(b)Department of Modern Physics, University of Science and Technology of China, Anhui; ^(c)Department of Physics, Nanjing University, Jiangsu; ^(d)High Energy Physics Group, Shandong University, Shandong, China
³³ Laboratoire de Physique Corpusculaire, Clermont Université and Université Blaise Pascal and CNRS/IN2P3, Aubiere Cedex, France
³⁴ Nevis Laboratory, Columbia University, Irvington NY, United States of America
³⁵ Niels Bohr Institute, University of Copenhagen, Kobenhavn, Denmark
³⁶ ^(a)INFN Gruppo Collegato di Cosenza; ^(b)Dipartimento di Fisica, Università della Calabria, Arcavata di Rende, Italy
³⁷ Faculty of Physics and Applied Computer Science, AGH-University of Science and Technology, Krakow, Poland
³⁸ The Henryk Niewodniczanski Institute of Nuclear Physics, Polish Academy of Sciences, Krakow, Poland
³⁹ Physics Department, Southern Methodist University, Dallas TX, United States of America
⁴⁰ Physics Department, University of Texas at Dallas, Richardson TX, United States of America
⁴¹ DESY, Hamburg and Zeuthen, Germany
⁴² Institut für Experimentelle Physik IV, Technische Universität Dortmund, Dortmund, Germany
⁴³ Institut für Kern- und Teilchenphysik, Technical University Dresden, Dresden, Germany
⁴⁴ Department of Physics, Duke University, Durham NC, United States of America
⁴⁵ SUPA - School of Physics and Astronomy, University of Edinburgh, Edinburgh, United Kingdom
⁴⁶ Fachhochschule Wiener Neustadt, Johannes Gutenbergstrasse 3, 2700 Wiener Neustadt, Austria
⁴⁷ INFN Laboratori Nazionali di Frascati, Frascati, Italy
⁴⁸ Fakultät für Mathematik und Physik, Albert-Ludwigs-Universität, Freiburg i.Br., Germany
⁴⁹ Section de Physique, Université de Genève, Geneva, Switzerland
⁵⁰ ^(a)INFN Sezione di Genova; ^(b)Dipartimento di Fisica, Università di Genova, Genova, Italy
⁵¹ Institute of Physics and HEP Institute, Georgian Academy of Sciences and Tbilisi State University, Tbilisi, Georgia
⁵² II Physikalisches Institut, Justus-Liebig-Universität Giessen, Giessen, Germany
⁵³ SUPA - School of Physics and Astronomy, University of Glasgow, Glasgow, United Kingdom
⁵⁴ II Physikalisches Institut, Georg-August-Universität, Göttingen, Germany
⁵⁵ Laboratoire de Physique Subatomique et de Cosmologie, Université Joseph Fourier and CNRS/IN2P3 and Institut National Polytechnique de Grenoble, Grenoble, France
⁵⁶ Department of Physics, Hampton University, Hampton VA, United States of America
⁵⁷ Laboratory for Particle Physics and Cosmology, Harvard University, Cambridge MA, United States of America
⁵⁸ ^(a)Kirchhoff-Institut für Physik, Ruprecht-Karls-Universität Heidelberg, Heidelberg; ^(b)Physikalisches Institut, Ruprecht-Karls-Universität Heidelberg, Heidelberg; ^(c)ZITI Institut für technische Informatik, Ruprecht-Karls-Universität Heidelberg, Mannheim, Germany
⁵⁹ Faculty of Science, Hiroshima University, Hiroshima, Japan
⁶⁰ Faculty of Applied Information Science, Hiroshima Institute of Technology, Hiroshima, Japan
⁶¹ Department of Physics, Indiana University, Bloomington IN, United States of America
⁶² Institut für Astro- und Teilchenphysik, Leopold-Franzens-Universität, Innsbruck, Austria
⁶³ University of Iowa, Iowa City IA, United States of America
⁶⁴ Department of Physics and Astronomy, Iowa State University, Ames IA, United States of America
⁶⁵ Joint Institute for Nuclear Research, JINR Dubna, Dubna, Russia
⁶⁶ KEK, High Energy Accelerator Research Organization, Tsukuba, Japan
⁶⁷ Graduate School of Science, Kobe University, Kobe, Japan
⁶⁸ Faculty of Science, Kyoto University, Kyoto, Japan
⁶⁹ Kyoto University of Education, Kyoto, Japan
⁷⁰ Instituto de Física La Plata, Universidad Nacional de La Plata and CONICET, La Plata, Argentina
⁷¹ Physics Department, Lancaster University, Lancaster, United Kingdom
⁷² ^(a)INFN Sezione di Lecce; ^(b)Dipartimento di Fisica, Università del Salento, Lecce, Italy
⁷³ Oliver Lodge Laboratory, University of Liverpool, Liverpool, United Kingdom

- ⁷⁴ Department of Physics, Jožef Stefan Institute and University of Ljubljana, Ljubljana, Slovenia
- ⁷⁵ Department of Physics, Queen Mary University of London, London, United Kingdom
- ⁷⁶ Department of Physics, Royal Holloway University of London, Surrey, United Kingdom
- ⁷⁷ Department of Physics and Astronomy, University College London, London, United Kingdom
- ⁷⁸ Laboratoire de Physique Nucléaire et de Hautes Energies, UPMC and Université Paris-Diderot and CNRS/IN2P3, Paris, France
- ⁷⁹ Fysiska institutionen, Lunds universitet, Lund, Sweden
- ⁸⁰ Departamento de Física Teórica C-15, Universidad Autónoma de Madrid, Madrid, Spain
- ⁸¹ Institut für Physik, Universität Mainz, Mainz, Germany
- ⁸² School of Physics and Astronomy, University of Manchester, Manchester, United Kingdom
- ⁸³ CPPM, Aix-Marseille Université and CNRS/IN2P3, Marseille, France
- ⁸⁴ Department of Physics, University of Massachusetts, Amherst MA, United States of America
- ⁸⁵ Department of Physics, McGill University, Montreal QC, Canada
- ⁸⁶ School of Physics, University of Melbourne, Victoria, Australia
- ⁸⁷ Department of Physics, The University of Michigan, Ann Arbor MI, United States of America
- ⁸⁸ Department of Physics and Astronomy, Michigan State University, East Lansing MI, United States of America
- ⁸⁹ ^(a)INFN Sezione di Milano; ^(b)Dipartimento di Fisica, Università di Milano, Milano, Italy
- ⁹⁰ B.I. Stepanov Institute of Physics, National Academy of Sciences of Belarus, Minsk, Republic of Belarus
- ⁹¹ National Scientific and Educational Centre for Particle and High Energy Physics, Minsk, Republic of Belarus
- ⁹² Department of Physics, Massachusetts Institute of Technology, Cambridge MA, United States of America
- ⁹³ Group of Particle Physics, University of Montreal, Montreal QC, Canada
- ⁹⁴ P.N. Lebedev Institute of Physics, Academy of Sciences, Moscow, Russia
- ⁹⁵ Institute for Theoretical and Experimental Physics (ITEP), Moscow, Russia
- ⁹⁶ Moscow Engineering and Physics Institute (MEPhI), Moscow, Russia
- ⁹⁷ Skobeltsyn Institute of Nuclear Physics, Lomonosov Moscow State University, Moscow, Russia
- ⁹⁸ Fakultät für Physik, Ludwig-Maximilians-Universität München, München, Germany
- ⁹⁹ Max-Planck-Institut für Physik (Werner-Heisenberg-Institut), München, Germany
- ¹⁰⁰ Nagasaki Institute of Applied Science, Nagasaki, Japan
- ¹⁰¹ Graduate School of Science, Nagoya University, Nagoya, Japan
- ¹⁰² ^(a)INFN Sezione di Napoli; ^(b)Dipartimento di Scienze Fisiche, Università di Napoli, Napoli, Italy
- ¹⁰³ Department of Physics and Astronomy, University of New Mexico, Albuquerque NM, United States of America
- ¹⁰⁴ Institute for Mathematics, Astrophysics and Particle Physics, Radboud University Nijmegen/Nikhef, Nijmegen, Netherlands
- ¹⁰⁵ Nikhef National Institute for Subatomic Physics and University of Amsterdam, Amsterdam, Netherlands
- ¹⁰⁶ Department of Physics, Northern Illinois University, DeKalb IL, United States of America
- ¹⁰⁷ Budker Institute of Nuclear Physics (BINP), Novosibirsk, Russia
- ¹⁰⁸ Department of Physics, New York University, New York NY, United States of America
- ¹⁰⁹ Ohio State University, Columbus OH, United States of America
- ¹¹⁰ Faculty of Science, Okayama University, Okayama, Japan
- ¹¹¹ Homer L. Dodge Department of Physics and Astronomy, University of Oklahoma, Norman OK, United States of America
- ¹¹² Department of Physics, Oklahoma State University, Stillwater OK, United States of America
- ¹¹³ Palacký University, RCPTM, Olomouc, Czech Republic
- ¹¹⁴ Center for High Energy Physics, University of Oregon, Eugene OR, United States of America
- ¹¹⁵ LAL, Univ. Paris-Sud and CNRS/IN2P3, Orsay, France
- ¹¹⁶ Graduate School of Science, Osaka University, Osaka, Japan
- ¹¹⁷ Department of Physics, University of Oslo, Oslo, Norway
- ¹¹⁸ Department of Physics, Oxford University, Oxford, United Kingdom
- ¹¹⁹ ^(a)INFN Sezione di Pavia; ^(b)Dipartimento di Fisica Nucleare e Teorica, Università di Pavia, Pavia, Italy
- ¹²⁰ Department of Physics, University of Pennsylvania, Philadelphia PA, United States of America
- ¹²¹ Petersburg Nuclear Physics Institute, Gatchina, Russia
- ¹²² ^(a)INFN Sezione di Pisa; ^(b)Dipartimento di Fisica E. Fermi, Università di Pisa, Pisa, Italy
- ¹²³ Department of Physics and Astronomy, University of Pittsburgh, Pittsburgh PA, United States of America
- ¹²⁴ ^(a)Laboratório de Instrumentação e Física Experimental de Partículas - LIP, Lisboa, Portugal; ^(b)Departamento de Física Teórica y del Cosmos and CAFPE, Universidad de Granada, Granada, Spain
- ¹²⁵ Institute of Physics, Academy of Sciences of the Czech Republic, Praha, Czech Republic
- ¹²⁶ Faculty of Mathematics and Physics, Charles University in Prague, Praha, Czech Republic

127 Czech Technical University in Prague, Praha, Czech Republic
 128 State Research Center Institute for High Energy Physics, Protvino, Russia
 129 Particle Physics Department, Rutherford Appleton Laboratory, Didcot, United Kingdom
 130 Physics Department, University of Regina, Regina SK, Canada
 131 Ritsumeikan University, Kusatsu, Shiga, Japan
 132 ^(a)INFN Sezione di Roma I; ^(b)Dipartimento di Fisica, Università La Sapienza, Roma, Italy
 133 ^(a)INFN Sezione di Roma Tor Vergata; ^(b)Dipartimento di Fisica, Università di Roma Tor Vergata, Roma, Italy
 134 ^(a)INFN Sezione di Roma Tre; ^(b)Dipartimento di Fisica, Università Roma Tre, Roma, Italy
 135 ^(a)Faculté des Sciences Ain Chock, Réseau Universitaire de Physique des Hautes Energies - Université Hassan II, Casablanca; ^(b)Centre National de l'Energie des Sciences Techniques Nucleaires, Rabat; ^(c)Université Cadi Ayyad, Faculté des sciences Semlalia Département de Physique, B.P. 2390 Marrakech 40000; ^(d)Faculté des Sciences, Université Mohamed Premier and LPTPM, Oujda; ^(e)Faculté des Sciences, Université Mohammed V, Rabat, Morocco
 136 DSM/IRFU (Institut de Recherches sur les Lois Fondamentales de l'Univers), CEA Saclay (Commissariat a l'Energie Atomique), Gif-sur-Yvette, France
 137 Santa Cruz Institute for Particle Physics, University of California Santa Cruz, Santa Cruz CA, United States of America
 138 Department of Physics, University of Washington, Seattle WA, United States of America
 139 Department of Physics and Astronomy, University of Sheffield, Sheffield, United Kingdom
 140 Department of Physics, Shinshu University, Nagano, Japan
 141 Fachbereich Physik, Universität Siegen, Siegen, Germany
 142 Department of Physics, Simon Fraser University, Burnaby BC, Canada
 143 SLAC National Accelerator Laboratory, Stanford CA, United States of America
 144 ^(a)Faculty of Mathematics, Physics & Informatics, Comenius University, Bratislava; ^(b)Department of Subnuclear Physics, Institute of Experimental Physics of the Slovak Academy of Sciences, Kosice, Slovak Republic
 145 ^(a)Department of Physics, University of Johannesburg, Johannesburg; ^(b)School of Physics, University of the Witwatersrand, Johannesburg, South Africa
 146 ^(a)Department of Physics, Stockholm University; ^(b)The Oskar Klein Centre, Stockholm, Sweden
 147 Physics Department, Royal Institute of Technology, Stockholm, Sweden
 148 Department of Physics and Astronomy, Stony Brook University, Stony Brook NY, United States of America
 149 Department of Physics and Astronomy, University of Sussex, Brighton, United Kingdom
 150 School of Physics, University of Sydney, Sydney, Australia
 151 Institute of Physics, Academia Sinica, Taipei, Taiwan
 152 Department of Physics, Technion: Israel Inst. of Technology, Haifa, Israel
 153 Raymond and Beverly Sackler School of Physics and Astronomy, Tel Aviv University, Tel Aviv, Israel
 154 Department of Physics, Aristotle University of Thessaloniki, Thessaloniki, Greece
 155 International Center for Elementary Particle Physics and Department of Physics, The University of Tokyo, Tokyo, Japan
 156 Graduate School of Science and Technology, Tokyo Metropolitan University, Tokyo, Japan
 157 Department of Physics, Tokyo Institute of Technology, Tokyo, Japan
 158 Department of Physics, University of Toronto, Toronto ON, Canada
 159 ^(a)TRIUMF, Vancouver BC; ^(b)Department of Physics and Astronomy, York University, Toronto ON, Canada
 160 Institute of Pure and Applied Sciences, University of Tsukuba, Ibaraki, Japan
 161 Science and Technology Center, Tufts University, Medford MA, United States of America
 162 Centro de Investigaciones, Universidad Antonio Narino, Bogota, Colombia
 163 Department of Physics and Astronomy, University of California Irvine, Irvine CA, United States of America
 164 ^(a)INFN Gruppo Collegato di Udine; ^(b)ICTP, Trieste; ^(c)Dipartimento di Fisica, Università di Udine, Udine, Italy
 165 Department of Physics, University of Illinois, Urbana IL, United States of America
 166 Department of Physics and Astronomy, University of Uppsala, Uppsala, Sweden
 167 Instituto de Física Corpuscular (IFIC) and Departamento de Física Atómica, Molecular y Nuclear and Departamento de Ingeniería Electrónica and Instituto de Microelectrónica de Barcelona (IMB-CNM), University of Valencia and CSIC, Valencia, Spain
 168 Department of Physics, University of British Columbia, Vancouver BC, Canada
 169 Department of Physics and Astronomy, University of Victoria, Victoria BC, Canada
 170 Waseda University, Tokyo, Japan
 171 Department of Particle Physics, The Weizmann Institute of Science, Rehovot, Israel
 172 Department of Physics, University of Wisconsin, Madison WI, United States of America
 173 Fakultät für Physik und Astronomie, Julius-Maximilians-Universität, Würzburg, Germany

- ¹⁷⁴ Fachbereich C Physik, Bergische Universität Wuppertal, Wuppertal, Germany
- ¹⁷⁵ Department of Physics, Yale University, New Haven CT, United States of America
- ¹⁷⁶ Yerevan Physics Institute, Yerevan, Armenia
- ¹⁷⁷ Domaine scientifique de la Doua, Centre de Calcul CNRS/IN2P3, Villeurbanne Cedex, France
- ^a Also at Laboratório de Instrumentação e Física Experimental de Partículas - LIP, Lisboa, Portugal
- ^b Also at Faculdade de Ciências and CFNUL, Universidade de Lisboa, Lisboa, Portugal
- ^c Also at Particle Physics Department, Rutherford Appleton Laboratory, Didcot, United Kingdom
- ^d Also at CPPM, Aix-Marseille Université and CNRS/IN2P3, Marseille, France
- ^e Also at TRIUMF, Vancouver BC, Canada
- ^f Also at Department of Physics, California State University, Fresno CA, United States of America
- ^g Also at Faculty of Physics and Applied Computer Science, AGH-University of Science and Technology, Krakow, Poland
- ^h Also at Department of Physics, University of Coimbra, Coimbra, Portugal
- ⁱ Also at Università di Napoli Parthenope, Napoli, Italy
- ^j Also at Institute of Particle Physics (IPP), Canada
- ^k Also at Department of Physics, Middle East Technical University, Ankara, Turkey
- ^l Also at Louisiana Tech University, Ruston LA, United States of America
- ^m Also at Group of Particle Physics, University of Montreal, Montreal QC, Canada
- ⁿ Also at Institute of Physics, Azerbaijan Academy of Sciences, Baku, Azerbaijan
- ^o Also at Institut für Experimentalphysik, Universität Hamburg, Hamburg, Germany
- ^p Also at Manhattan College, New York NY, United States of America
- ^q Also at School of Physics and Engineering, Sun Yat-sen University, Guanzhou, China
- ^r Also at Academia Sinica Grid Computing, Institute of Physics, Academia Sinica, Taipei, Taiwan
- ^s Also at High Energy Physics Group, Shandong University, Shandong, China
- ^t Also at Section de Physique, Université de Genève, Geneva, Switzerland
- ^u Also at Departamento de Física, Universidade de Minho, Braga, Portugal
- ^v Also at Department of Physics and Astronomy, University of South Carolina, Columbia SC, United States of America
- ^w Also at KFKI Research Institute for Particle and Nuclear Physics, Budapest, Hungary
- ^x Also at California Institute of Technology, Pasadena CA, United States of America
- ^y Also at Institute of Physics, Jagiellonian University, Krakow, Poland
- ^z Also at Department of Physics, Oxford University, Oxford, United Kingdom
- ^{aa} Also at Institute of Physics, Academia Sinica, Taipei, Taiwan
- ^{ab} Also at Department of Physics, The University of Michigan, Ann Arbor MI, United States of America
- ^{ac} Also at DSM/IRFU (Institut de Recherches sur les Lois Fondamentales de l'Univers), CEA Saclay (Commissariat à l'Energie Atomique), Gif-sur-Yvette, France
- ^{ad} Also at Laboratoire de Physique Nucléaire et de Hautes Energies, UPMC and Université Paris-Diderot and CNRS/IN2P3, Paris, France
- ^{ae} Also at Department of Physics, Nanjing University, Jiangsu, China
- * Deceased